EKSAKTA
Journal of Sciences and Data Analysis

E-ISSN: 2720-9326
P-ISSN: 2716-0459

DOI :10.20885/EKSAKTA.vol6.iss2.art1

Ni-decorated biochar from palm leaves waste as low-cost photocatalyst for dye degradation of methyl orange

Galih Dwiki Ramanda[1*], Is Fatimah[2], Suresh Sagadevan[3], Mohd Rafie Bin Johan[4]

[1,] Institut Teknologi dan Kesehatan Muhammadiyah Kalimantan Barat
[2,] Department of Chemistry, Faculty of Mathematics and Natural Sciences, Universitas Islam Indonesia
[3,4] Universiti Malaya

[*] *Corresponding author: galih@itekesmukalbar.ac.id*

Abstract: Photocatalytic oxidation is one of the methods in the advanced oxidation process. The method depends on several factors to be effective in application, one of these is the cost-effectivity and sustainability. The intent of this research work is to synthesize low-cost photocatalyst by using waste: palm leaves ash. Lignocellulosic as a structural compenent found in palm leaves has the potential for various applications, including as a catalyst for wastewater treatment. The Ni-biochar (Ni-BC) photocatalyst based on nickel nanoparticles was synthesized by using palm leaves under pyrolysis method on two varied Ni content; 10 and 30 % wt to get Ni10-BC and Ni30-BC, respectively. Various characterization techniques consist of XRD, SEM, and VSM were conducted, meanwhile the photocatalytic activity for methyl orange photodegradation was employed as activity testing. Results showed that single nickel nanoparticles dispersed on biochar structure are appeared by XRD measurement. The porous structure of materials is derived, with the magnetism of 9.64 emu/g and 3.87 emu/g for Ni content of 10 and 30 % wt., respectively. The fabricated Ni-BC samples showed excellent photoactivity represented by 50.01 and 74.73% of the degradation efficency towards methyl orange by Ni10-BC and Ni30-BC, respectively. A persuasive mechanism and kinetics are well presented. The kinetics study expressed the fitness of the degradation that follow pseudo-first order kinetics.

Keywords: Biochar, Methyl orange, Nickel nanoparticle, Photocatalytic, Pyrolysis

Introduction

The rapid expansion of industrial activities has resulted in the discharge of synthetic dyes into aquatic ecosystems, where their persistence and toxicity pose significant environmental and health risks [1]. Among these pollutants, methyl orange (MO), an azo dye widely used in textile and printing industries, has been frequently detected in wastewater streams due to its high stability and resistance to conventional treatment methods [2]. The presence of MO not only imparts strong coloration to water bodies, thereby reducing light penetration and photosynthetic activity, but also releases potentially carcinogenic aromatic amines upon incomplete degradation. Such challenges highlight the urgent need for effective and sustainable remediation strategies capable of achieving complete mineralization of MO and related organic pollutants [3], [4].

E-ISSN: 2720-9326
P-ISSN: 2716-0459
DOI :

Photocatalytic oxidation, a widely studied branch of advanced oxidation processes, has emerged as a promising strategy for the degradation of synthetic dyes such as methyl orange [5]. In this process, a photocatalyst activated under light irradiation generates reactive oxygen species, primarily hydroxyl (•OH) and superoxide ($\bullet O_2^-$) radicals, which are capable of breaking down the azo bonds (–N=N–) and aromatic rings of MO into less harmful compounds [6], [7]. Despite its effectiveness, the large-scale application of photocatalytic systems is often restricted by the high cost of conventional semiconductor catalysts, limited raw material availability, and challenges related to stability and reusability. To overcome these barriers, biochar-based photocatalysts have recently gained attention as cost-effective carbonaceous materials that can serve as a support for photoactive metals or metal oxides [8]. Through their inherent adsorption capacity and porous structure, biochar materials can enhance the interaction between pollutants and active sites, thereby accelerating photocatalytic reactions and improving overall degradation efficiency [9].

Lignocellulosic biomass has emerged as a promising precursor for the development of carbon-based functional materials due to its abundance, renewable nature, and intrinsic structural features. Agricultural residues such as palm leaves, rich in lignocellulosic components, are often discarded as waste despite their high potential for value-added applications. The utilization of such waste not only contributes to waste management and circular economy practices but also provides a cost-effective approach to developing catalyst supports or active photocatalytic materials [10], [11].

Nickel-based photocatalysts are of particular interest due to their ability to improve charge separation and facilitate redox reactions during photocatalysis. The incorporation of Ni nanoparticles onto a biochar matrix enhances the surface active sites and electron mobility, thereby suppressing electron–hole recombination [12]. Under light irradiation, the excitation of the biochar–Ni system generates electron–hole pairs, where photogenerated electrons (e^-) can migrate toward the Ni sites and participate in the reduction of dissolved oxygen to form superoxide radicals ($\bullet O_2^-$), while the photogenerated holes (h^+) oxidize water or hydroxide ions to produce hydroxyl radicals (•OH). These reactive oxygen species are the key oxidants responsible for the mineralization of organic pollutants. Moreover, the intrinsic graphitic domains of biochar provide π–π conjugated networks that facilitate electron transfer, while its porous structure increases the dispersion and stabilization of Ni nanoparticles. The synergy between the biochar support and Ni species thus contributes to enhanced photocatalytic activity and durability compared with pristine biochar or conventional Ni catalysts [13].

Building upon these insights, the present study aims to synthesize and evaluate a low-cost photocatalyst derived from palm leaves biochar impregnated with nickel nanoparticle. The Ni-BC composites were prepared via pyrolysis with varying nickel loadings of 10 and 30 wt%. The photocatalytic performance of the materials was subsequently assessed through the degradation of methyl orange as a model organic pollutant. This work not only addresses the dual challenges of waste valorization and environmental remediation but also provides a sustainable approach toward developing

E-ISSN: 2720-9326
P-ISSN: 2716-0459
DOI :

efficient photocatalysts for photocatalytic oxidation processes in wastewater treatment applications.

Materials and Methods

Materials

Palm leaves were obtained from palm agricultural areas in West Kalimantan, Indonesia, and used as the biomass source. Nickel (II) chloride ($NiCl_2 \cdot 6H_2O$) and methyl orange (MO) were purchased from Merck (Darmstadt, Germany). PT Samator, Indonesia, supplied ultra-high purity nitrogen (N_2) gas. An electric oven was used for drying, while a tubular furnace equipped with a continuous N_2 flow was employed for pyrolysis. The photocatalytic experiments were conducted using a UV lamp reactor system, and the concentration of methylene orange was analyzed using a UV–Vis pectrophotometer.

Preparation of Nickel-Supported Biochar (Ni-BC)

The preparation of nickel-supported biochar followed a modified impregnation–pyrolysis method. Palm leaves were washed with distilled water, dried at 105 °C for 24 h, chopped into small pieces, and impregnated with $NiCl_2$ solution for 24 h, with nickel loadings of 10 and 30 wt.%. After impregnation, the samples were oven-dried at 110 °C for 12 h and pyrolyzed in a tubular furnace at 600 °C for 1 h under continuous N_2 flow to obtain Ni-BC. From the Ni content variation, the samples were encoded ad Ni10-BC and Ni30-BC, respectively.

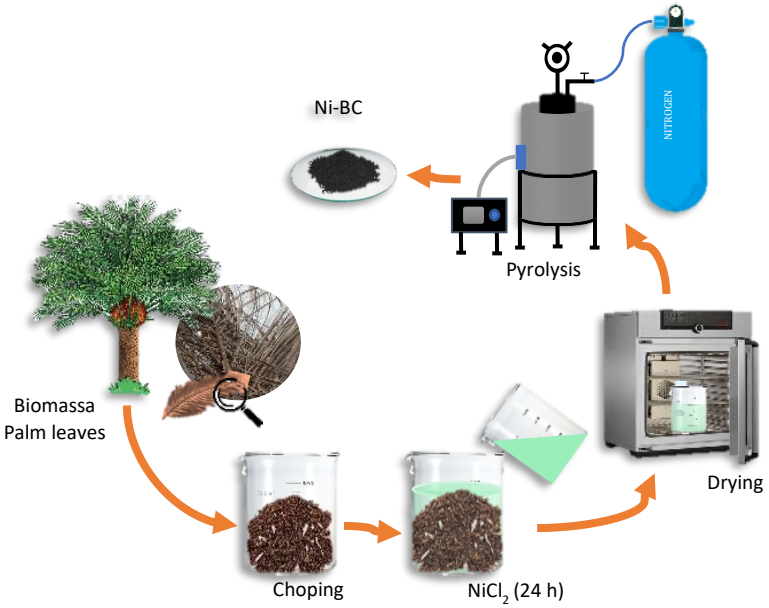

Figure 1. Schematic Representation of Ni-BC Preparatio

Characterization of Ni-BC

The physicochemical properties of Ni-BC were analyzed using several techniques. The crystalline structure was characterized by X-ray diffraction (XRD, Shimadzu X-6000) equipped with a Ni-filtered Cu-Kα radiation source (λ = 0.154060 nm). Surface

E-ISSN: 2720-9326
P-ISSN: 2716-0459
DOI :

morphology was observed using Field Emission Scanning Electron Microscopy (FE-SEM, Phenom™ XL Desktop). Magnetic properties were analyzed using Vibrating Sample Magnetometry (VSM, LakeShore 7407, USA).

Photocatalytic Activity Test

Photocatalytic degradation experiments were performed by dispersing 0.2 g of Ni-BC into 100 mL of MO solution (50 ppm). The mixture was exposed irradiated with a UV lamp (Philips, 365 nm) (UV Photocatalytic Oxidation Reactor Na under continuous stirring for 2 h. Aliquots of 3 mL were collected at 0, 15, 30, 45, 60, 90, and 120 min, centrifuged to separate the catalyst, and analyzed using a UV–Vis spectrophotometer (PerkinElmar Lambda 35). Control experiments were carried out without catalyst and without UV irradiation to verify the photocatalytic effect of Ni-BC.

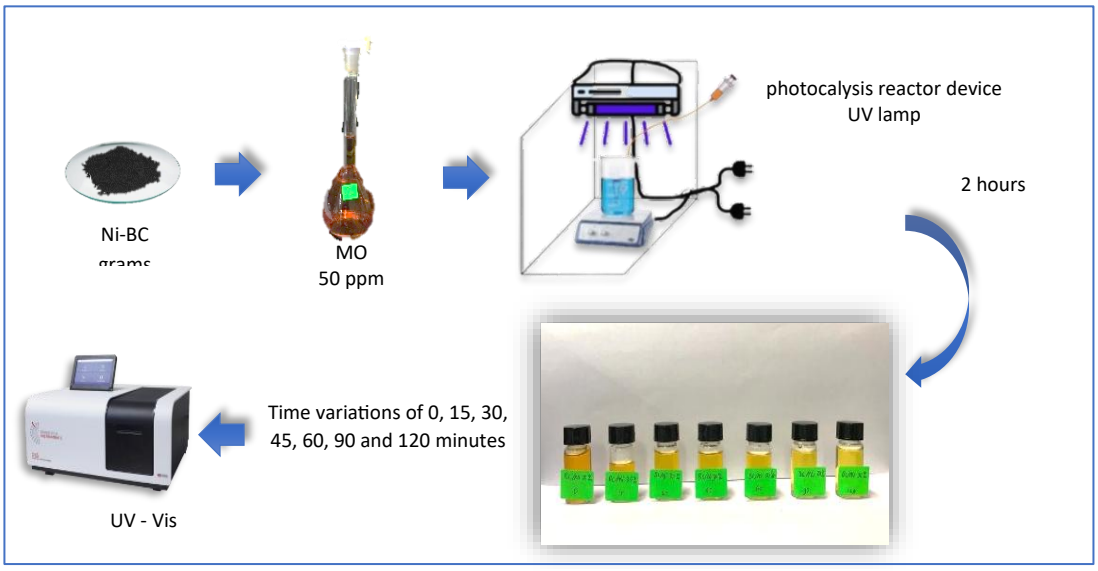

Figure 2. Ni10-BC and Ni30-BC UV Lamp Photocatalysis Test

Results and Discussions

Physicochemical Characterization Ni-BC

The XRD patterns of BC and Ni-BC are shown in Figure 3. The BC sample exhibits a broad diffraction peak at 2θ = 20°–30°, corresponding to the (002) plane of graphitic carbon, which indicates the amorphous nature and small crystallite size of the biochar structure. Minor peaks observed at around 26° and 27° are attributed to cristobalite and calcite, reflecting the presence of residual inorganic minerals derived from the agricultural precursor. In contrast, the Ni-BC sample displays distinct diffraction peaks at 2θ = 45°, 52.3°, and 77.4°, which correspond to the (111), (200), and (220) planes of face-centered cubic (FCC) nickel (JCPDS No. 03-1051). These reflections confirm the successful incorporation and uniform dispersion of Ni nanoparticles on the biochar matrix. The presence of metallic Ni enhances the crystalline structure and provides active sites that may improve the material's catalytic and adsorption performance [14][15].

E-ISSN: 2720-9326
P-ISSN: 2716-0459

DOI :

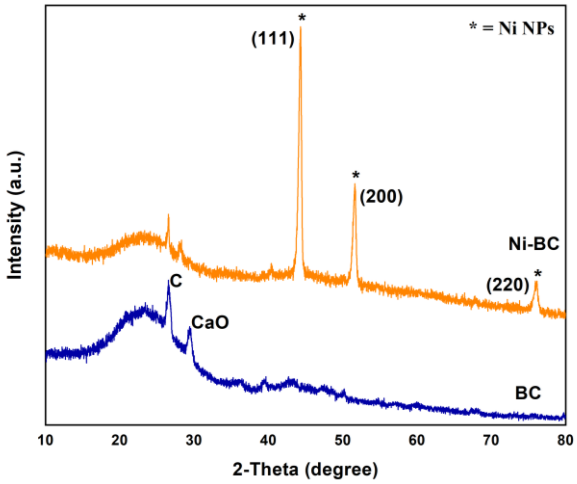

Figure 3. XRD patterns of BC and Ni-BC

The surface morphology of BC and Ni-BC was further examined using SEM to support the XRD results. The types of minerals from the Ni-BC nanocomposites with different nickel contents (10% and 30%) are shown in Figure 4. The SEM images reveal that the Ni10-BC composite exhibits a relatively porous biochar structure with visible dispersion of Ni nanoparticles (NiNPs), as indicated by the bright spots on the surface [16]. At higher magnification, the nickel particles are more clearly observed, suggesting their successful incorporation into the biochar matrix. In contrast, the Ni30-BC composite demonstrates a denser surface morphology with a greater distribution of NiNPs, which indicates a higher degree of metal loading [17]. The corresponding EDX spectra (Figure 5) confirm the presence of nickel along with other elements typically found in biochar such as C, O, Si, K, and Ca, supporting the successful impregnation of nickel into the biochar framework [18]. Similar findings have been reported in previous studies, where increasing metal loading enhanced particle dispersion and surface coverage of the support material [19].

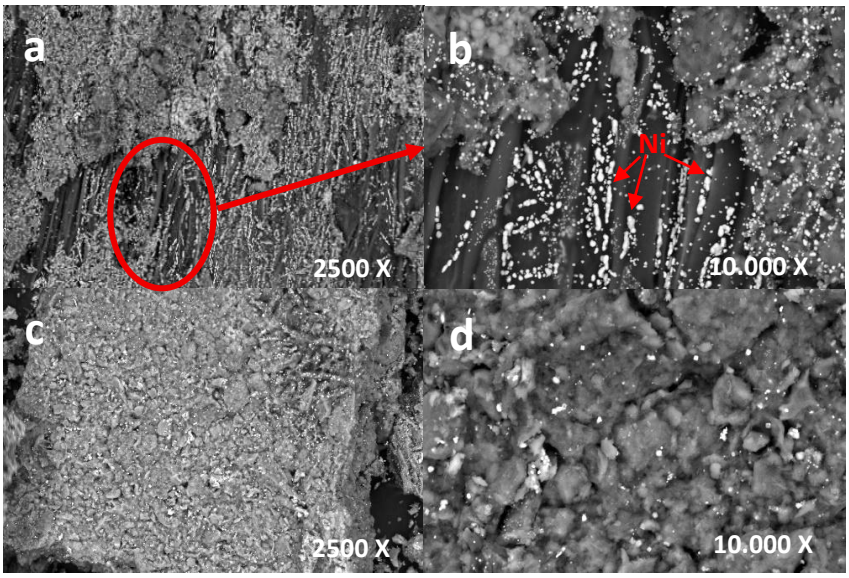

Figure 4. SEM-EDX images of (a-b) Ni10-BC with different magnification (c-d) Ni30-BC with different magnifications

E-ISSN: 2720-9326
P-ISSN: 2716-0459
DOI :

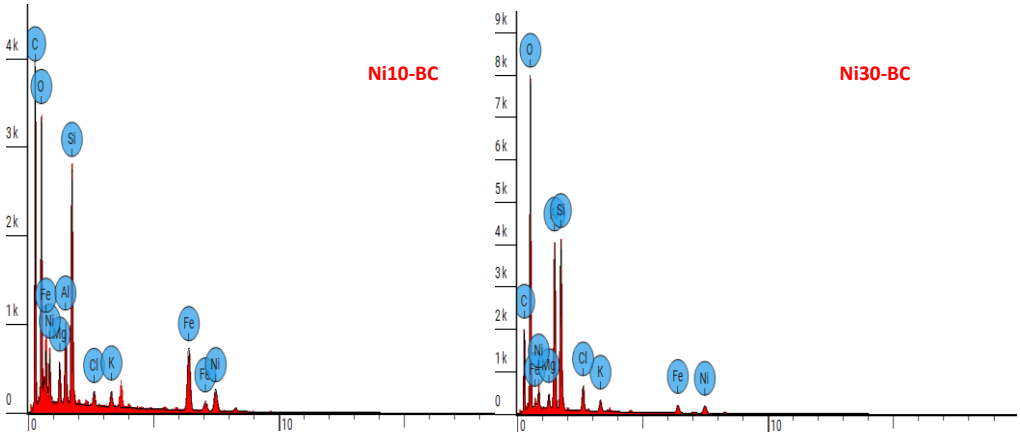

Figure 5. EDX spectra of Ni10-BC and Ni30-BC

The magnetic attractivity of Ni-BC is confirmed by VSM. The plot shows that Ni10-BC and Ni30-BC expressed superparamagnetic characteristics with a saturation magnetization value (Ms) of approximately 9.64 emu g−1 and 3.87 emu g−1. The higher Ms value of Ni10-BC compared to Ni30-BC indicates that excessive nickel loading may lead to particle agglomeration and reduced magnetic response, consistent with previous findings on Ni-loaded biochar composites [20]. Furthermore, both samples exhibited negligible coercivity and remanence, confirming their superparamagnetic nature. This property allows Ni-BC composites to be easily attracted by an external magnetic field, as illustrated in Figure 6, facilitating efficient separation and recovery from aqueous systems. Such a feature is highly advantageous for catalytic and environmental applications, where reusability and ease of separation are essential.

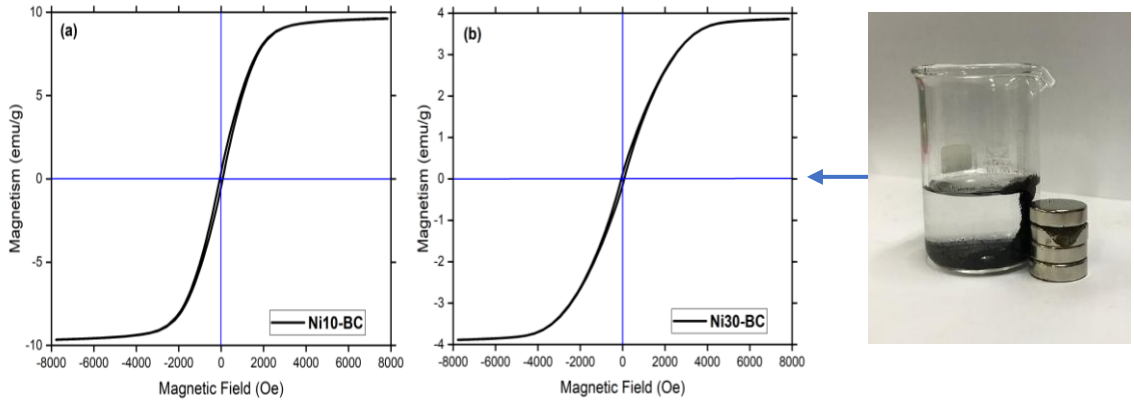

Figure 6. (a) Hysteresis loop of Ni10-BC (b) Hysteresis loop of Ni30-BC, and photographs showing the magnetic separation of Ni-BC particles in aqueous solution

Photocatalytic Activity Test

The photocatalytic performance of Ni-BC nanocomposites was evaluated through the degradation of MO under UV irradiation, as shown in Figure 7. The UV–Vis absorption spectra indicate that in the absence of a catalyst (photolysis, Fig. 7a), only a slight decrease in absorbance was observed, confirming that MO is relatively stable under UV light alone. When pristine BC was used (Fig. 7b), a minor improvement in degradation was observed, attributed to its limited adsorption and light absorption capacity. In

E-ISSN: 2720-9326
P-ISSN: 2716-0459
DOI :

contrast, the introduction of Ni significantly enhanced the degradation process, with Ni10-BC (Fig. 7c) and Ni30-BC (Fig. 7d) exhibiting a progressive decrease in absorption intensity, suggesting improved photocatalytic activity with increasing Ni loading. The kinetic curves of C/C_0 versus time (Fig. 7e) further confirm this trend, showing that the degradation rate of Ni30-BC was markedly higher than that of Ni10-BC, BC, and photolysis. After 120 minutes of UV irradiation, the degradation efficiencies (Fig. 7f) reached 74.73% for Ni30-BC, 50.01% for Ni10-BC, 31.94% for BC, and only 8.67% for photolysis. The superior performance of Ni30-BC can be attributed to the higher number of Ni active sites that enhance charge transfer and promote the generation of reactive oxygen species, thereby accelerating MO degradation. Conversely, the lower efficiency of Ni10-BC and BC suggests that insufficient metal loading or lack of active sites limits photocatalytic activity. These results are consistent with previous studies reporting that optimal incorporation of transition metals into biochar improves photocatalytic degradation while minimizing electron–hole recombination. [21], [22].

Table 1. Comparison of Ni-BC Photocatalysts for Methyl Orange (MO) Degradation

Photocatalyst (biochar-based)	Method	Treatment time (min)	Degradation effifiency toward MO (%)	Reference
Ni/NiO–biochar (biowaste-derived)	Carbothermal	100	99.00	[23]
TiO2/biochar (walnut-shell)	Hydrolysis	60	96.88	[24]
Ag–TiO_2/biochar (walnut shell)	Calcination	60	97.48	[25]
ZnO/biochar (lignin-based carbons)	Carbonization	30	96.90	[26]
Cu/Cu_2O/BC (rice husk)	Impregnation	60	95.00	[27]
Ni10-BC and Ni30-BC (palm leaves)	Pyrolysis	120	50.01 and74.73	This work

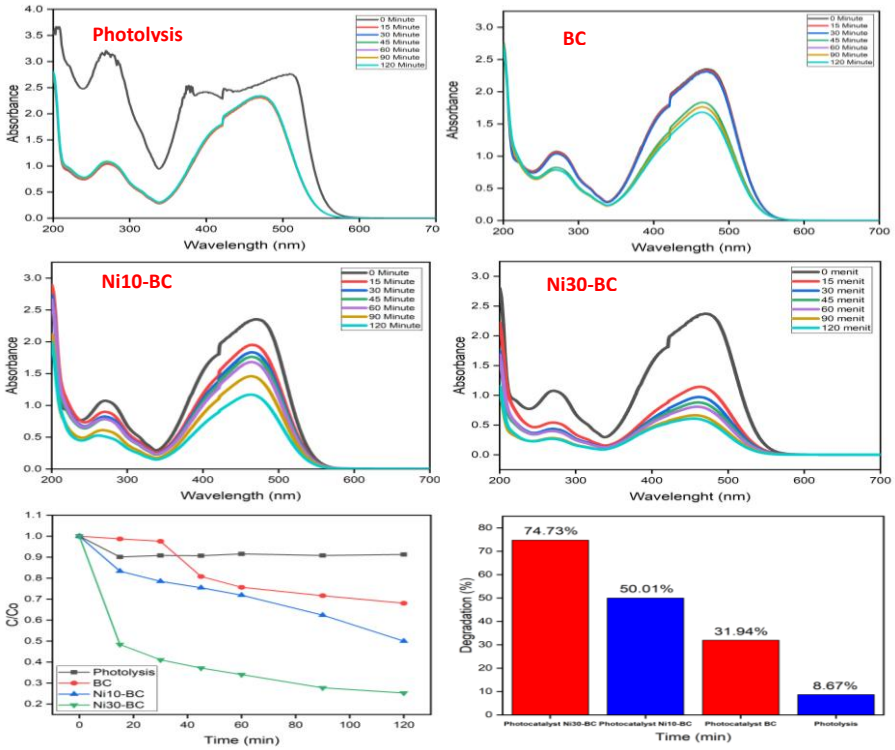

Figure 7. Photocatalytic degradation of methylene orange: UV–Vis absorption spectra of (a) photolysis, (b) BC, (c) BC10-Ni, and (d) Ni30-Ni; (e) kinetic curves of C/C_0 versus time; and (f) degradation efficiency after 120 min

E-ISSN: 2720-9326
P-ISSN: 2716-0459
DOI :

The comparative photocatalytic performance of biochar-supported catalysts toward MO degradation is summarized in Table 1. Reported efficiencies for metal oxide–immobilized biochars, such as TiO_2/BC, ZnO/BC, Ag–TiO_2/BC, and Cu/Cu_2O/BC, are notably high, typically achieving over 95% degradation within 30–100 minutes of irradiation. In contrast, the Ni10-BC and Ni30-BC catalysts synthesized in this study from palm leaf waste exhibited lower degradation efficiencies of 50.01% and 74.73% after 120 minutes, respectively.

This comparison highlights several intrinsic limitations of Ni–biochar systems relative to TiO_2- or ZnO-based composites. Unlike TiO_2 and ZnO, which possess wide band gaps, high photo-response, and superior charge mobility, Ni-loaded biochar tends to suffer from lower crystallinity, smaller surface area, and higher electron–hole recombination rates. These factors collectively restrict its photocatalytic performance. Moreover, the non-semiconducting nature of metallic Ni reduces light absorption efficiency under UV irradiation, thereby limiting the generation of reactive oxygen species compared to oxide-based catalysts.

Nevertheless, the Ni30-BC catalyst still demonstrates a promising level of activity within the context of Ni-based biochar systems. The use of palm leaves as a carbon source offers an environmentally friendly and low-cost alternative to conventional supports. To overcome current limitations, several optimization strategies are recommended: enhancing Ni nanoparticle dispersion through controlled impregnation, tuning pyrolysis temperature to improve graphitization and surface area, and introducing co-dopants such as TiO_2, ZnO, or CeO_2 to promote charge separation and light absorption.

Therefore, although Ni–biochar derived from palm leaves exhibits lower photocatalytic efficiency than oxide–biochar composites, it provides a sustainable and low-cost platform that can be further engineered to achieve or even match the high (>90%) degradation efficiencies reported in literature. This work establishes a promising foundation for developing environmentally friendly photocatalysts from underutilized agricultural residues.

Kinetics Studies

The kinetic behavior of MO degradation over Ni-BC composites was evaluated using the pseudo-first-order kinetic model, and the corresponding plots are presented in Figure 6. The results clearly demonstrate that the degradation kinetics of MO can be well described by the pseudo-first-order equation, as evidenced by the good linearity of the fitted plots. Both composites exhibited good linearity with correlation coefficients (R^2) above 0.91, confirming that the pseudo-first-order equation is suitable to describe the degradation process. Interestingly, the Ni30-BC composite exhibited a higher rate constant ($k = 0.0115\ min^{-1}$, $R^2 = 0.9189$) compared to Ni10-BC ($k = 0.00578\ min^{-1}$, $R^2 = 0.9653$), indicating that increasing the Ni loading enhanced the photocatalytic performance [28].

The improvement in activity at higher Ni content can be attributed to the greater availability of photocatalytic active sites, which promote more efficient interaction between Ni particles and the biochar surface. The higher density of Ni nanoparticles

E-ISSN: 2720-9326
P-ISSN: 2716-0459
DOI :

facilitates stronger light absorption, where the absorbed light promotes radical generation to oxidize target molecules [29]. In addition, the intimate contact between Ni and biochar may generate a synergistic effect, where biochar acts as an electron mediator, suppressing charge recombination and thus accelerating the degradation process.

Although excessive metal loading in many cases often leads to particle agglomeration or pore blocking, the Ni30-BC composite in this study maintained sufficient surface accessibility and dispersion of Ni species, as suggested by the characterization results. Consequently, the Ni30-BC content provided an optimal balance between electron–hole separation, photon utilization, and surface reactivity, resulting in superior kinetic performance compared to the Ni10-BC counterpart [30].

These results are consistent with previous studies reporting that an increased concentration of transition metals on carbon-based supports can significantly enhance catalytic degradation efficiency when the particles remain well-dispersed and accessible [31]. Thus, the findings suggest that tailoring the Ni loading plays a crucial role in optimizing the photocatalytic activity of biochar-based nanocomposites.

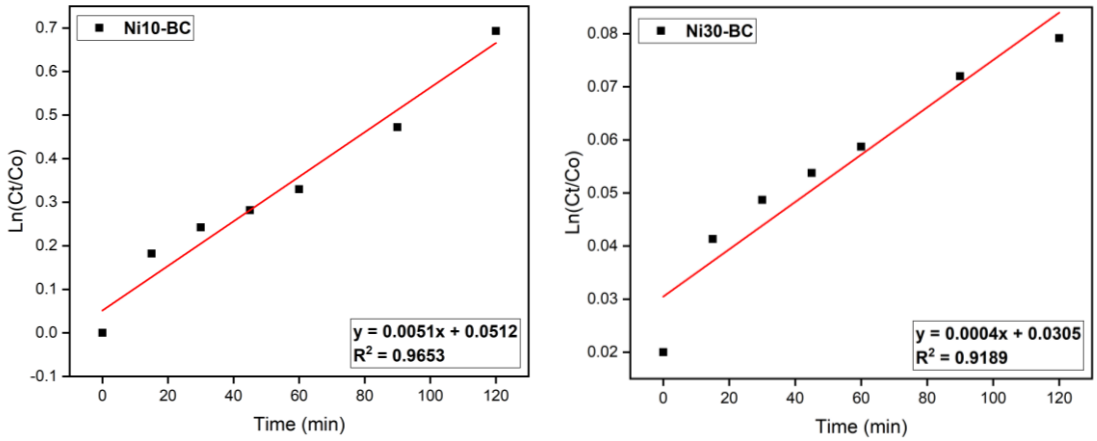

Figure 7. Pseudo-first-order kinetic plots for the photocatalytic degradation of methyl orange using (a) Ni10-BC and (b) Ni30-BC

Conclusion

The synthesis of nickel-supported biochar nanocomposites (Ni-BC) using palm leaf waste through pyrolysis at 600 °C for 1 h was successfully achieved, producing Ni10-BC and Ni30-BC. SEM analysis confirmed the incorporation and uniform dispersion of Ni particles within the biochar matrix, while VSM results indicated a magnetic property of 9.64 emu/g. The photocatalytic activity of the composites was evaluated for methylene orange degradation, where Ni30-BC exhibited higher performance, achieving 77.74% degradation after 120 min of irradiation. Kinetic analysis revealed that both samples followed pseudo-first-order behavior, with rate constants (k) of 0.0115 min^{-1} for Ni30-BC and 0.00578 min^{-1} for Ni10-BC, corresponding to half-lives ($t_1/_2$) of 60.5 min and 120.0 min, respectively. These findings suggest that Ni-BC nanocomposites, particularly at higher Ni loadings, have significant potential as efficient photocatalysts for removing

E-ISSN: 2720-9326
P-ISSN: 2716-0459
DOI :

organic pollutants from wastewater, offering a promising route for environmental remediation and wastewater treatment applications.

Acknowledgement

The author sincerely thanks Prof. Dr. Is Fatimah, M.Si., for their valuable guidance and support. Special appreciation is also extended to Dr. Suresh Sagadevan, and Prof. Ruey-An Doong for their constructive input and collaboration. Research support from the Laboratory of Materials for Energy and Environment, Chemistry Department, Universitas Islam Indonesia, as well as facilities provided by NANOCAT, University of Malaya, is gratefully acknowledged.

References

[1] A. Das and A. Dey, "P-Nitrophenol-Bioremediation using potent Pseudomonas strain from the textile dye industry effluent," *J. Environ. Chem. Eng.*, vol. 8, no. 4, p. 103830, 2020.

[2] M. Shafqat, A. Khalid, T. Mahmood, M. T. Siddique, J. I. Han, and M. Y. Habteselassie, "Evaluation of bacteria isolated from textile wastewater and rhizosphere to simultaneously degrade azo dyes and promote plant growth," *J. Chem. Technol. Biotechnol.*, vol. 92, no. 10, pp. 2760–2768, 2017, doi: 10.1002/jctb.5357.

[3] K. Rehman *et al.*, "Effect of Reactive Black 5 azo dye on soil processes related to C and N cycling," *PeerJ*, vol. 2018, no. 5, pp. 1–14, 2018, doi: 10.7717/peerj.4802.

[4] D. A. Bopape, B. Ntsendwana, and F. D. Mabasa, "Photocatalysis as a pre-discharge treatment to improve the effect of textile dyes on human health: A critical review," *Heliyon*, vol. 10, no. 20, p. e39316, 2024, doi: 10.1016/j.heliyon.2024.e39316.

[5] X. Yang *et al.*, "Photocatalytic oxidation aging significantly enhanced the interaction between microplastics and methyl orange," *Total Environ. Eng.*, vol. 4, p. 100025, 2025, doi: https://doi.org/10.1016/j.teengi.2025.100025.

[6] F. Mohammadkhani, M. Montazer, and M. Latifi, "Microwave absorption and photocatalytic properties of magnetic nickel nanoparticles/recycled PET nanofibers web," *J. Text. Inst.*, vol. 110, no. 11, pp. 1606–1614, Nov. 2019, doi: 10.1080/00405000.2019.1612501.

[7] I. Fatimah, H. K. Wijayanti, G. D. Ramanda, M. Tamyiz, R. A. Doong, and S. Sagadevan, "Nanocomposite of Nickel Nanoparticles-Impregnated Biochar from Palm Leaves as Highly Active and Magnetic Photocatalyst for Methyl Violet Photocatalytic Oxidation," *Molecules*, vol. 27, no. 20, pp. 1–13, 2022, doi: 10.3390/molecules27206871.

[8] E. Dwi Ana Santosa, M. Tamyiz, S. Sagadevan, A. Hidayat, I. Fatimah, and R. Doong, "Stable and magnetically separable nanocomposite prepared from bauxite mining tailing waste as catalyst in wet peroxidation of tetracycline," *Results Chem.*, vol. 4, p. 100451, 2022, doi: https://doi.org/10.1016/j.rechem.2022.100451.

[9] Y. Fu, Y. Yi, Y. Wang, Y. Diao, Z. Diao, and Z. Chen, "A comprehensive review of modified biochar-based advanced oxidation processes for environmental pollution remediation: efficiency, mechanism, toxicity assessment," *J. Environ. Manage.*, vol. 387, p. 125872, 2025, doi: https://doi.org/10.1016/j.jenvman.2025.125872.

[10] G. D. Ramanda, A. Allwar, M. Tamyiz, I. Fatimah, and R. A. Doong, "Nickel/Biochar from Palm Leaves Waste as Selective Catalyst for Producing Green Diesel by Hydrodeoxygenation of Vegetable Oil," *Bull. Chem. React. Eng. Catal.*, vol. 18, no. 1, pp. 25–36, 2023, doi: 10.9767/BCREC.16403.

[11] R. Wardhani and Y. Rahadian, "Sustainability strategy of Indonesian and Malaysian palm oil industry: a qualitative analysis," *Sustain. Accounting, Manag. Policy J.*, vol. 12, no. 5, pp. 1077–1107, May 2021, doi: 10.1108/SAMPJ-07-2020-0259.

[12] N. Zahir, V. Rajangam, S. S. Kalanur, S. I. Nikitenko, and B. G. Pollet, "Harnessing

E-ISSN: 2720-9326
P-ISSN: 2716-0459
DOI :

Nickel-Based Photocatalysts for CO2 Conversion and Hydrogen Production – A Review," *Energy Environ. Mater.*, vol. 8, no. 4, 2025, doi: 10.1002/eem2.70014.

[13] L. El Gaini, "Enhancing solar-driven photocatalysis: Synergistic integration of biochar, semiconductors, and magnetic materials for degrading organic pollutants," *Desalin. Water Treat.*, vol. 320, p. 100798, 2024, doi: https://doi.org/10.1016/j.dwt.2024.100798.

[14] M. F. Arkaan, R. F. Ekaputri, I. Fatimah, and A. Kamari, "Physicochemical and photocatalytic activity of hematite/biochar nanocomposite prepared from Salacca skin waste," *Sustain. Chem. Pharm.*, vol. 16, p. 100261, 2020.

[15] F. Taghizadeh, "The study of structural and magnetic properties of NiO nanoparticles," *Opt. Photonics J.*, vol. 6, no. 8, pp. 164–169, 2016.

[16] D. E. and H. Annal Therese, "Hierarchical Nickel nanowire synthesis using polysorbate 80 as capping agent," *Appl. Surf. Sci.*, vol. 449, pp. 48–54, 2018, doi: https://doi.org/10.1016/j.apsusc.2017.12.176.

[17] Zulqarnain *et al.*, "Low-temperature steam reforming of toluene as a biomass tar model compound over biochar-supported catalysts," *Biochar*, vol. 7, no. 1, p. 42, 2025, doi: 10.1007/s42773-025-00437-3.

[18] M. Prasad, N. Tzortzakis, and N. McDaniel, "Chemical characterization of biochar and assessment of the nutrient dynamics by means of preliminary plant growth tests," *J. Environ. Manage.*, vol. 216, pp. 89–95, 2018, doi: 10.1016/j.jenvman.2017.04.020.

[19] S. Azeem *et al.*, "Surface engineered sustainable nanocatalyst with improved coke resistance for dry methane reforming to produce hydrogen," *Process Saf. Environ. Prot.*, vol. 187, pp. 962–973, 2024, doi: https://doi.org/10.1016/j.psep.2024.05.033.

[20] L. Kong, J.-F. Lv, Y. Li, and Y.-C. Quan, "Effects of coexisting nickel ions on properties of spinel synthesized in wastewater containing chromium and insight into the effect mechanism," *Sep. Sci. Technol.*, vol. 59, no. 4, pp. 660–669, Mar. 2024, doi: 10.1080/01496395.2024.2335335.

[21] L. Kanku, K. O. Badmus, and F. Wewers, "Biochar-Supported Titanium Oxide for the Photocatalytic Treatment of Orange II Sodium Salt," 2024. doi: 10.3390/applnano5030013.

[22] I. Fatimah *et al.*, "Highly active photocatalyst of nickel oxide nanoparticles green-synthesized using Tinosphora cordifolia-plant extract for photocatalytic oxidation of tetracycline," *Environ. Nanotechnology, Monit. Manag.*, vol. 22, no. March, p. 100968, 2024, doi: 10.1016/j.enmm.2024.100968.

[23] P. P. Mon, P. P. Cho, L. Chandana, V. V. S. S. Srikanth, G. Madras, and S. Ch, "Biowaste-derived Ni/NiO decorated-2D biochar for adsorption of methyl orange," *J. Environ. Manage.*, vol. 344, p. 118418, 2023, doi: https://doi.org/10.1016/j.jenvman.2023.118418.

[24] L. Lu, R. Shan, Y. Shi, S. Wang, and H. Yuan, "A novel TiO2/biochar composite catalysts for photocatalytic degradation of methyl orange," *Chemosphere*, vol. 222, pp. 391–398, 2019, doi: 10.1016/j.chemosphere.2019.01.132.

[25] R. Shan *et al.*, "Photocatalytic degradation of methyl orange by Ag/TiO2/biochar composite catalysts in aqueous solutions," *Mater. Sci. Semicond. Process.*, vol. 114, no. April, p. 105088, 2020, doi: 10.1016/j.mssp.2020.105088.

[26] Z. Tang, Y. Yang, and W. Wei, "Efficient Catalytic Degradation of Methyl Orange by Various ZnO-Doped Lignin-Based Carbons.," *Molecules*, vol. 29, no. 8, Apr. 2024, doi: 10.3390/molecules29081817.

[27] A. Photocatalytic *et al.*, "Preparation of Cu / Cu 2 O / BC and Its Performance in," 2024.

[28] I. Fatimah, G. D. Ramanda, S. Sagadevan, Suratno, M. Tamyiz, and R. an Doong, "One-pot synthesis of nickel nanoparticles-embedded biochar and insight on adsorption, catalytic oxidation and photocatalytic oxidation of dye," *Case Stud. Chem. Environ. Eng.*, vol. 10, no. February, p. 100767, 2024, doi: 10.1016/j.cscee.2024.100767.

[29] H. Zhang *et al.*, "Removal of methyl orange from aqueous solutions by adsorption on cellulose hydrogel assisted with Fe2O3 nanoparticles," *Cellulose*, vol. 24, no. 2, pp. 903–914, 2017, doi: 10.1007/s10570-016-1129-1.

E-ISSN: 2720-9326
P-ISSN: 2716-0459

DOI :

[30] S. Pradhan, N. S. Anuraag, N. Jatav, I. Sinha, and N. K. Prasad, "Magnetic Ni@C nanoadsorbents for methyl orange removal from water," *Environ. Sci. Pollut. Res.*, vol. 30, no. 56, pp. 118634–118646, 2023, doi: 10.1007/s11356-023-30588-4.

[31] J. Tafjord *et al.*, "Transition-Metal Nanoparticle Catalysts Anchored on Carbon Supports via Short-Chain Alginate Linkers," *ACS Appl. Nano Mater.*, vol. 4, no. 4, pp. 3900–3910, Apr. 2021, doi: 10.1021/acsanm.1c00294.